J|A|C|S
ARTICLES
Published on Web 08/09/2006

Solid Memory: Structural Preferences in Group 2 Dihalide Monomers, Dimers, and Solids

Kelling J. Donald and Roald Hoffmann*

Contribution from the Department of Chemistry and Chemical Biology, Baker Laboratory, Cornell University, Ithaca, New York 14853

Received April 22, 2006; E-mail: rh34@cornell.edu

Abstract: The link between structural preferences in the monomers, dimers, and extended solid-state structures of the group 2 dihalides (MX_2: M = Be, Mg, Ca, Sr, Ba and X = F, Cl, Br, I) is examined theoretically. The question posed is how well are geometric properties of the gas-phase MX_2 monomers and lower order oligomers "remembered" in the corresponding MX_2 solids. Significant links between the bending in the MX_2 monomers and the D_{2h}/C_{3v} M_2X_4 dimer structures are identified. At the B3LYP computational level, the monomers that are bent prefer the C_{3v} triply bridged geometry, while the rigid linear molecules prefer a D_{2h} doubly bridged structure. Quasilinear or floppy monomers show, in general, only a weak preference for either the D_{2h} or the C_{3v} dimer structure. A frontier orbital perspective, looking at the interaction of monomer units as led by a donor−acceptor interaction, proves to be a useful way to think about the monomer−oligomer relationships. There is also a relationship between the structural trends in these two (MX_2 and M_2X_4) series of molecular structures and the prevalent structure types in the group 2 dihalide solids. The most bent monomers condense to form the high coordination number fluorite and $PbCl_2$ structure types. The rigidly linear monomers condense to form extended solids with low coordination numbers, 4 or 6. The reasons for these correlations are explored.

Introduction

Chemistry is well-supplied with instances in which expectations of simplicity are met with real complexity, with experimental observations forcing us to revise ideas on which our intuition is built. The bending observed in the group 2 dihalides is among the most interesting examples of such seemingly counterintuitive behavior. It is now well-known that not all the group 2 dihalide molecules have linear minimum energy structures. In the series MX_2 (M ≡ Be, Mg, Ca, Sr, Ba; X ≡ F, Cl, Br, I), the molecules CaF_2, SrF_2, $SrCl_2$, and all the BaX_2 structures are bent.[1−2]

Simple valence bond and molecular orbital models, such as the traditional valence shell electron pair repulsion (VSEPR) model[3] and simple Walsh diagrams,[4] fail to predict this behavior. Since the discovery in the 1960s of this unexpected bending in the group 2 dihalides,[5] various attempts have been made to explain it.[6−16] For the most part, these explanations have been based on classical electrostatic core-polarization models[7,9,11,15a,16] or hybridization models that take account of the empty $(n-1)d$ energy level in the heavier metal atoms.[8,10−15] Over the past decade or so, a consensus has gradually emerged that, in fact, both core-polarization and hybridization significantly affect the bonding and structural preferences in these systems.[1,2,12]

An interesting structural diversity has been observed experimentally and computationally in the series of dimers of the group 2 dihalides, $(MX_2)_2$, as well. The Be_2X_4 and Mg_2X_4 dimers have a D_{2h} minimum energy structure with two bridging halides, while Ca_2F_4, Sr_2X_4, and Ba_2X_4, X = F, Cl, feature a C_{3v} minimum energy geometry with three bridging halides (Figure 1).[1,17−21]

(1) Hargittai, M. *Chem. Rev.* **2000**, *100*, 2233.
(2) Kaupp, M. *Angew. Chem., Int. Ed.* **2001**, *40*, 3535.
(3) (a) Sidgwick, N. V.; Powell, H. M. *Proc. R. Soc. London, Ser. A* **1940**, *176*, 153. (b) Gillespie, R. J.; Nyholm, R. S. *Quart. Rev.* **1957**, *11*, 339. (c) Gillespie, R. J.; Hargittai, I. *The VSEPR Model of Molecular Geometry*; Allyn & Bacon, Boston, 1991.
(4) (a) Walsh, A. D. *J. Chem. Soc.* **1953**, 2260, 2266. (b) Cotton, F. A.; Wilkinson, G. *Advanced Inorganic Chemistry*, 5th ed; Wiley and Sons: New York, 1988; pp 22−32.
(5) (a) Wharton, L.; Berg, R. A.; Klemperer, W. *J. Chem. Phys.* **1963**, *39*, 2023. (b) Büchler, A.; Stauffer, J. L.; Klemperer, W. *J. Chem. Phys.* **1964**, *40*, 3471. (c) Büchler, A.; Stauffer, J. L.; Klemperer, W. *J. Am. Chem. Soc.* **1964**, *86*, 4544.
(6) (a) Hayes, E. F. *J. Phys. Chem.* **1966**, *70*, 3740. (b) Gole, J. L.; Siu, A. K. Q.; Hayes, E. F. *J. Chem. Phys.* **1973**, *58*, 857.
(7) (a) Eliezer, I. *Theor. Chim. Acta* **1970**, *18*, 77. (b) Eliezer, I.; Reger, A. *Theor. Chim. Acta* **1972**, *26*, 283.
(8) (a) Coulson, C. A. *Nature (London)* **1969**, *221*, 1106. (b) Coulson, C. A. *Isr. J. Chem.* **1973**, *11*, 683.
(9) Guido M.; Gigli, G. *J. Chem. Phys.* **1976**, *65*, 1397.
(10) Kilmenko, N. M.; Musaev, D. G.; Charkin, O. P. *Russ. J. Inorg. Chem.* **1984**, *29*, 639; *Zh. Neorg. Khim.* **1984**, *29*, 1114.
(11) DeKock, R. L.; Peterson, M. A.; Timmer, L. K.; Baerends, E. J.; Vernooijs, P. *Polyhedron* **1990**, *9*, 1919; **1991**, *10*, 1965 (erratum).
(12) Szentpály, L. v.; Schwerdtfeger, P. *Chem. Phys. Lett.* **1990**, *170*, 555.
(13) (a) Hassett, D. M.; Marsden, C. J. *J. Chem. Soc., Chem. Commun.* **1990**, 667. (b) Hassett, D. M.; Marsden, C. J. *J. Mol. Struct.* **1995**, *346*, 249.
(14) Seijo, L.; Barandiarán, Z.; Huzinaga, S. *J. Chem. Phys.* **1991**, *94*, 3762.
(15) (a) Kaupp, M.; Schleyer, P. v. R.; Stoll, H.; Preuss, H. *J. Am. Chem. Soc.* **1991**, *113*, 6012. (b) Kaupp, M.; Schleyer, P. v. R. *J. Am. Chem. Soc.* **1992**, *114*, 491.
(16) Donald, K. J.; Mulder, W. H.; Szentpály, L. v. *J. Chem. Phys.* **2003**, *119*, 5423.
(17) Guido, M.; Gigli, G. *J. Chem. Phys.* **1977**, *66*, 3920.
(18) Gigli, G. *J. Chem. Phys.* **1990**, *93*, 5224. Mg_2Cl_4 was examined much earlier in ref 17.
(19) Pogrebnaya, T. P.; Sliznev, V. V.; Solomonik, V. G. *Russ. J. Coord. Chem.* **1997**, *23*, 461; *Koord. Khim.* **1997**, *23*, 498.
(20) Levy, J. B.; Hargittai, M. *J. Phys. Chem. A.* **2000**, *104*, 1950.
(21) Hargittai, M. *Struct. Chem.* **2005**, *16*, 33.

10.1021/ja062817j CCC: $33.50

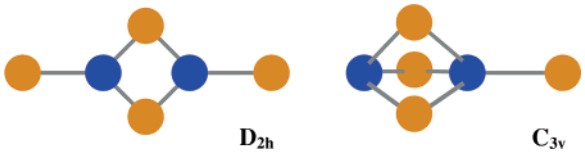

Figure 1. Minimum-energy structural isomers of the groups 2 dihalide dimers.

A question that arises naturally is whether there is a link between the linear/bent structural variation in the monomer and the D_{2h}/C_{3v} geometrical preference in the dimer. For the systems examined computationally to date, it has been found, in fact, that the monomers that are bent prefer a C_{3v} dimeric structure, while the linear monomers tend to adopt the D_{2h} dimer geometry.

Five years ago, Levy and Hargittai performed density functional calculations on six different isomers of Ca_2X_4, Sr_2X_4, and Ba_2X_4, X = F and Cl.[20] They identified for those six systems a correlation between the linear(bent) geometry preference in the monomers and the $D_{2h}(C_{3v})$ geometry preference in the dimer. Furthermore, they provided computational evidence that, for Ca_2F_4, Sr_2F_4, Ba_2F_4 and $BaCl_2$, the D_{2h} conformation is not even a local minimum on the potential energy surface.[20] To the best of our knowledge, however, the Sr and Ba dibromide and diiodide dimers are yet to be fully characterized experimentally or studied using reliable computational methods. Interested in this linear(bent) $D_{2h}(C_{3v})$ correlation, we have examined a more complete series of the dimer structures to understand better the correspondence between the structural preferences in all 20 monomers and their dimers.

The main subject of this paper is, however, a broader one. We want to know the factors influencing structural proclivities and choices made not only in the dimer but also in higher order oligomers and the extended solids. Ultimately, we would like to better understand how the significantly ionic solids are built up from their simpler building blocks and how well they may *remember* the structural peculiarities of those building blocks.

A systematic analysis of a series of clusters, beginning at the molecule and moving from dimer to trimer etc., would help to answer these questions. Such a study would enable us to see if (and help us to understand how) monomer geometries influence cluster and solid structures. We can do a good job on the dimers, but trimers, tetramers, and other oligomers are likely to be found in a veritable multitude of isomeric local minima. That variability by and large disappears when one gets to the periodic extended solids. So, in this work we will bypass the trimer and higher order oligomer geometries and move directly to examining the solids themselves.

The crystal structures of the solids have been extensively discussed in the literature.[22−24] The structure types exhibited by nearly all the group 2 metal dihalide MX_2 crystals are very well-known: for instance, the rutile structure of MgF_2 and the CaF_2 (fluorite) structure are routinely depicted and analyzed in modern textbooks of structural chemistry.[24] We will show these structures later in this paper.

Structural maps have been developed (for the group 2 dihalides as well as other MX_2 crystal structures) correlating atomic properties of M and X atoms and the MX_2 structure types they adopt.[22,23] These maps have been quite useful in helping solid-state chemists make sense of why a certain combination of M and X atoms may prefer one particular MX_2 structure type over another.

This kind of empirical structural analysis has been carried out for gas-phase molecules, as well. Thus, the bending in group 2 dihalides has been rationalized based on differences in atomic parameters such as valence-orbital radii[25] or atomic softness.[12,26] As far as we know, however, there has been no attempt to make contact between the arguments explaining geometric variations in the gas phase and the rationalization of the structure profiles (structure types, coordination numbers, etc.) in the solid phases of these dihalides.[27]

In the present work, we take a first step toward making this connection. We begin by optimizing geometries for the group 2 dihalide monomers and a range of dimer geometries. Correlations between preferred geometries and structural trends in the monomer and dimer structures are identified and examined. The tendencies that are observed in both sets of structures are then compared with the structure type variations in the corresponding MX_2 solids at ambient conditions.

At the end, we discuss how the framework of understanding within which structural variations in the gas phase (monomers and dimers) has been rationalized may more generally inform our understanding of bonding in the solid-phase structures.

Theoretical Methods

Optimized geometries of the monomer and dimer (C_{3v} and D_{2h}) structures of the group 2 dihalides have been obtained using the B3LYP[28] density functional method and the following basis sets: the 6-311+G* all-electron basis set was used for Be and Mg; for the larger metal atoms (Ca, Sr, and Ba), we have used the 10-valence electron effective core MWB (WB MEFIT) pseudopotentials and 6s6p5d basis sets developed by the German (Stuttgart and Erlangen) groups.[29] The optimized monomer geometries are sensitive to the *d* orbital contraction scheme, and uncontracted *d*-functions have been recommended for the heavier metals.[15a,20,29] For this reason, the 6s6p5d basis set with uncontracted *d* polarization functions have been used. The cc-pVTZ all-electron basis set of Dunning et al.[30] has been employed for F and Cl. The latter is unavailable for I and is very expensive computationally for Br; for those halides we have employed the (7-valence electron) effective core MWB pseudopotentials and basis sets.

In addition to being less expensive computationally, the B3LYP method has been shown by Levy and Hargittai[20] to afford reliable geometric and frequency data for monomers and dimers of CaX_2, SrX_2, and BaX_2 (X = F, Cl). For comparison, and to augment the data set available for the dimers, all structures have been optimized at the second-order Møller−Plesset, MP2, level of theory, as well, using the said basis sets.[31] All our theoretical calculations have been carried out using the Gaussian 03 suite of programs.[32]

(22) Mooser, E.; Pearson W. B. *Acta Crystallogr.* **1959**, *12*, 1015.
(23) Burdett, J. K.; Price, G. D.; Price S. L. *Phys. Rev. B* **1981**, *24*, 2903.
(24) (a) Müller, U. *Inorganic Structural Chemistry*; John Wiley and Sons: Chichester, 1992. (b) Wells, A. F. *Structural Inorganic Chemistry*, 3rd ed.; Clarendon Press: Oxford, 1962.
(25) Andreoni, W.; Galli, G.; Tosi, M. *Phys. Rev. Lett.* **1985**, *55*, 1734.
(26) Szentpály, L. v. *J. Phys. Chem. A* **2002**, *106*, 11945.
(27) We should mention, however, the work of Wilson and Madden; they examined and compared the gas-phase monomer, dimer, and crystal structures of $BeCl_2$: Wilson, M.; Madden, P. A. *Mol. Phys.* **1997**, *92*, 197.
(28) Becke, A. D. *J. Chem. Phys.* **1993**, *98*, 5648. Lee, C.; Yang, W.; Parr, R. G. *Phys. Rev. B* **1988**, *37*, 785.
(29) Kaupp, M.; Schleyer, P. v. R.; Stoll, H.; Preuss, H. *J. Chem. Phys.* **1991**, *94*, 1360.
(30) (a) Woon, D. E.; Dunning, T. H. *J. Chem. Phys.* **1993**, *98*, 1358. (b) Kendall, R. A.; Dunning, T. H.; Harrison, R. J. *J. Chem. Phys.* **1992**, *96*, 6796. (c) Dunning, T. H. *J. Chem. Phys.* **1989**, *90*, 1007.
(31) Head-Gordon, M.; Head-Gordon, T.; *Chem. Phys. Lett.* **1994**, *220*, 122 and references therein.
(32) Frisch, M. J. et al.*Gaussian 03*, revision B.04; Gaussian, Inc.: Pittsburgh, PA, 2003.

Table 1. Structural and Energy Data for the Group 2 Dihalides: Experimental and Computed (B3LYP) Bond Distances r and Angles Θ,[a,b] Computed Linearization Energies $E_{lin} = (E(D_{\infty h}) - E(C_{2v}))$, and Computed Bending Force Constants k_{lin} for the Optimized $D_{\infty h}$ (Linear) Structures

	r/Å[a,c]		Θ/deg[a]		E_{lin}/eV	k_{lin}/eV rad^{-2} [d]
MX_2	this work	expt	this work	expt	this work	this work
BeF_2	1.377	1.374(4)	180	180		8.717
$BeCl_2$	1.800	1.791(5)	180	180		7.225
$BeBr_2$	1.961	1.932(11)	180	180		5.751
BeI_2	2.172		180	180		5.221
MgF_2	1.759	1.746	180	180		5.788
$MgCl_2$	2.186	2.162(5)	180	180		6.225
$MgBr_2$	2.344	2.308(8)	180	180		5.120
MgI_2	2.552		180	180		4.439
CaF_2	1.996		142.8	142 (1)	0.04	−2.090
$CaCl_2$	2.470	2.455(8)	180	180		0.510
$CaBr_2$	2.640	2.592(20)	180	180		1.114
CaI_2	2.857	2.822(13)	180	180		1.151
SrF_2	2.130		128.8	108	0.14	−3.051
$SrCl_2$	2.633	2.606(8)	152.6	143.3(34)	0.01	−0.702
$SrBr_2$	2.821	2.748(13)	180	q-linear[b]		0.089
SrI_2	3.040	2.990	180	180		0.525
BaF_2	2.258		118.0	100	0.34	−4.631
$BaCl_2$	2.773		126.9	100; 120(10)	0.13	−2.571
$BaBr_2$	2.973	2.899(7)	130.4	137.1(49)	0.07	−2.280
BaI_2	3.210	3.130	133.9	137.6(9)[f]	0.04	−1.739

[a] Experimental geometries are from refs 1, 36−38, and 43. In ref 1, M. Hargittai has provided an excellent summary of experimental and ab initio geometries that have been obtained for these systems. The experimental errors in brackets are in units of the last significant figure; so, e.g., 137.1(49) ↔ 137.1 ± 4.9. Bond lengths and bond angles obtained at the MP2 and QCISD computational levels are included in Table S.1. [b] For the so-called quasilinear molecules, the experimental numbers can differ significantly (especially results obtained by matrix isolation IR techniques). For example, in ref 42, $\Theta(CaF_2) = 142°$ (argon matrix) and 131° (krypton matrix). For earlier estimates of Θ for $SrCl_2$, $BaBr_2$, and BaI_2, see ref 41. [c] See refs 40 and 44. In some instances we have been unable to locate reliable experimental values that have been adjusted[40] for comparison with the computed geometries. [d] 1 mdyne Å^{-1} = 6.241 51 × (r_{linear}/Å)^2 eV/radian^2, where r_{linear}, the optimized M−X bond distance in the linear geometry, is in Å units. The values of r_{linear} and the computed (B3LYP) force constants in mdyne/Å units are given in Table S.2 of the Supporting Information. [e] See ref 15a. [f] See ref 35.

Frequency analysis on the dihalide dimers was necessary in order to characterize the structures we obtained. Levy and Hargittai have already pointed out that at the B3LYP level the default fine grid calculations lead to too many imaginary frequencies and retention of translational contributions.[20] To avoid this pitfall, we have adopted the ultrafine grid, as well, for our frequency calculations.

Structural Preferences in the Group 2 Dihalide Monomers

The unanticipated bending of the group 2 dihalides is the focus of continued interest in these molecules. The structural variation in the series is quite significant, with bond angles ranging roughly from 100° to 180° (Table 1), with increased bending as the metal ion gets larger and the halides get smaller (for recent experimental and computational data, see ref 1).

Yielding to a desire to impose order on this small and interesting world of MX_2 molecules, workers have adopted a three-tier classification scheme, categorizing them as linear, quasilinear, and bent. The so-called quasilinear or floppy molecules are those found experimentally to be linear (or bent), but having a relatively low potential energy barrier to bending (or linearization).[2,14] The question of which molecules to put in this category is not easy to answer, as it depends on how conservatively one defines the cutoff linearization (bending) energy. CaF_2, $CaCl_2$, $SrCl_2$, and $SrBr_2$ are structures typically described as quasilinear. Among these, $SrBr_2$ exhibits the lowest potential energy barrier (0.001 eV)[15a] and is probably the most deserving of the quasilinear label.[1,33] Computed linearization energies (the energy required to make the bent minimum energy structure linear) are shown in column 6 of Table 1. For further discussion on variations in the MX_2 linearization energies and the concept of quasilinearity, see refs 2, 14, 33, and 34.

Aside from a comparison of the potential energy barriers separating the linear and the bent geometries, the relative flexibility of the structures may be assessed by the theoretical bending force constants. The preferred geometry and rigidity (or flexibility) of the MX_2 molecules are characterized by the sign and magnitude of the bending force constant of the linearized structure

$$k_{lin}(\pi) = \left(\frac{\partial^2 U(\Theta)}{\partial \Theta^2}\right)_{\Theta=\pi} = \left(\frac{\partial^2 U(\theta)}{4\partial \theta^2}\right)_{\theta=\pi/2}$$

Here, $U(\Theta)$ is the molecular potential energy expressed as a function of the X−M−X bond angles, Θ (=2θ). k_{lin} is positive for linear molecules and is negative for the bent ones. Further, the magnitude of k is a measure of the flexibility of the molecule: the more flexible the molecule is, the smaller the magnitude of k. Hence, the most rigid molecules in the linear (or bent) geometries will have the largest positive (or negative) k_{lin} values. Very flexible systems, such as $SrBr_2$, will have relatively small (positive or negative) bending force constants. A set of k_{lin} values from this work is provided in column 7 of Table 1. The bending force constants listed in Table 1 were obtained directly from our Gaussian 03 calculations (in mdynes Å^{-1} units) and converted to units of eV rad^{-2} (see footnote d of Table 1 for the conversion factor). See Table S.2 (Supporting Information) for values obtained previously by Kaupp et al.[15a] We will return to these quantities later on in the discussion.

Computational (B3LYP) and experimental geometries[1,35−43] of the alkaline earth dihalide molecules are listed in Table 1, as well. Additionally, ab initio data that we have obtained at the MP2 and QCISD levels and values obtained by Kaupp et

(33) Hargittai, M.; Kolonits, M.; Knausz, D.; Hargittai, I. *J. Chem. Phys.* **1992**, *96*, 8980.
(34) The term quasilinear is somewhat misleading, implying linearity for all these structures; so, we have accepted the more colloquial but comprehensive description: floppy. The boundaries separating the floppy and the "genuinely" linear or bent molecules are not defined rigorously. Kaupp recently adopted a partitioning scheme based on linearization energies. He described as quasilinear all molecules with energy changes < 4 kJ mol^{-1} (~0.04 eV) when deviated by more than 20° around the linear geometry. By that scheme, all the Ca dihalides, $SrCl_2$, $SrBr_2$, SrI_2, and BaI_2 qualify as quasilinear.
(35) Spiridonov, V. P.; Gershikov, A. G.; Altman, A. B.; Romanov, G. V.; Ivanov, A. A. *Chem. Phys. Lett.* **1981**, *77*, 41. The so-called harmonic equilibrium BaI_2 bond distance and bond angle reported by Spiridonov et al. are r_e^h = 3.150(7) Å and Θ_e^h = 148.0(9)°. The parameters given in Table 1 are from ref 1. In that work, r_e is estimated from the experimental r_g distance obtained by Spiridonov et al. Further, the thermally averaged bond angle, Θ_a = 137.6(9)°, from Spiridonov et al. was selected instead of Θ_e^h.
(36) Giricheva, N. I.; Girichev, G. V.; Girichev, A. G.; Shlykov, S. A. *Struct. Chem.* **2000**, *11*, 313.
(37) Hargittai, M.; Kolonits, M.; Schultz, G. *J. Mol. Struct.* **2001**, *567−568*, 241.
(38) Réffy, B.; Kolonits, M.; Hargittai, M. *J. Phys. Chem. A* **2005**, *109*, 8379.
(39) In ref 1, M. Hargittai has provided a comprehensive review of the experimental structural studies done on the group 2 dihalides before the year 2000. For specific references to experimental studies on individual molecules in the series, see Table 7 of that work.

al.[15a] (QCISD) are included in the Supporting Information (Table S.1). The bending trend is very well established at all three computational levels, with increased bending as the cation gets softer (larger) and the anion gets harder (smaller).[26]

The density functional (B3LYP) bond lengths and angles show reasonable qualitative agreement with the MP2 and QCISD levels of theory and experiment (Table S.1). The B3LYP method tends to exaggerate the bending when compared to those two methods but shows the best overall agreement with the experimental geometries for the dihalides (Table S.1). It must be emphasized here, however, that, for *floppy* (or *quasilinear*) molecules with shallow bending potentials, such as CaF_2, $SrBr_2$, and BaI_2 ($0.00\ \text{eV} < E_{\text{lin}} \leq 0.04\ \text{eV}$),[2,34] the experimental errors are quite large typically. On the computational side, the geometries and bending potentials of floppy molecules are particularly sensitive to the choice of model chemistry (computational method and basis set).[1,2,12,15,44]

The anomalous structural variation in the group 2 dihalide compounds has been extensively discussed in the literature, and a comprehensive review, dedicated in part to models rationalizing the bending trend, has been provided by Kaupp.[2] For the larger cations, the significant bending in the monomer (small Θ in Table 1) is favored, since the $(n-1)d$ orbitals are low-lying and sd^x hybridization is cheaper, compared to sp^x hybridization.[2,8] Following a classical electrostatic description of the molecules, it has been shown that polarization interactions (including charge-induced dipole and higher order interactions) between the softer cations and the harder anions are enhanced by the bending. And they play a key role in stabilizing the bent Ca, Sr, and Ba dihalide systems as well (see ref 16 and references therein).

Having summarized the structural and energetic data for the monomers, we will turn our attention next to the dihalide dimers.

Group 2 Dihalide Dimers: Structural Preferences

As mentioned above, there is an evident correlation between the structures of the MX_2 molecules and their stable dimers.[1] The monomers that are linear dimerize preferentially in the D_{2h} geometry, but the bent monomers tend to form a triply bridged C_{3v} dimeric structure (Figure 1). This conclusion has been arrived at slowly and piecewise, however, several groups having contributed over the past decade, examining various parts of the series of dimers experimentally and at various levels of theory.[1,17−20,45,46] Furthermore, quantum mechanical or accurate experimental data are unavailable for a few dimers, including Sr_2I_4 and Ba_2I_4.

In the present work, 10 *possible* dimer geometries have been studied (see Figure 2), including (i) the D_{2h} and (ii) the C_{3v} isomers already mentioned (Figure 1). Geometry optimizations

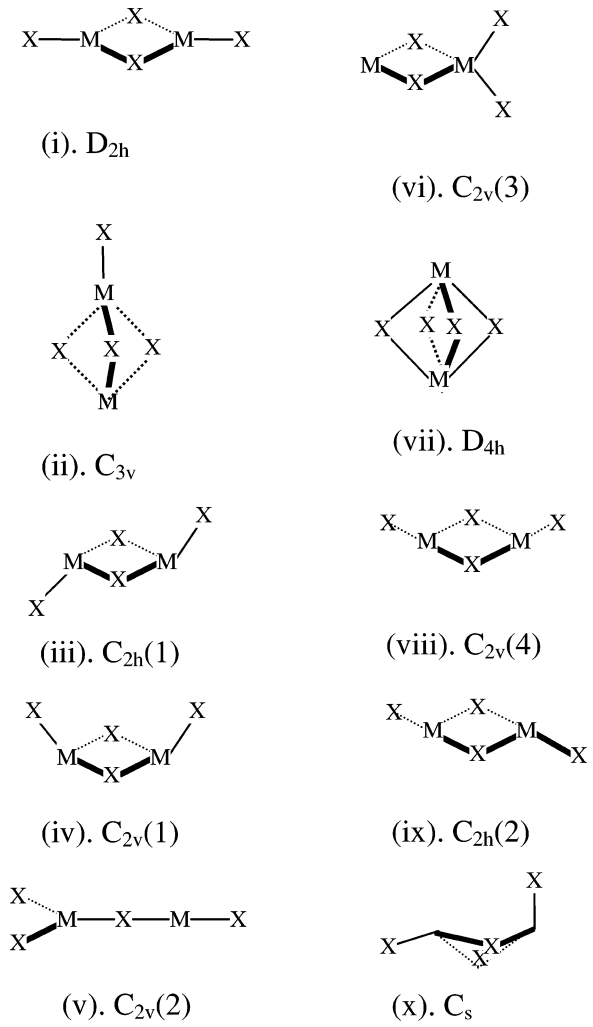

Figure 2. Possible geometries of the metal dihalide dimers.

have been performed at the B3LYP computational level at reasonable starting points for all 10 geometries (Figure 2). The energies of isomers (ii) to (x) (Figure 2) relative to the D_{2h} structure, $\Delta E = E(\text{isomer}) - E(D_{2h})$, and the number of imaginary frequencies for all the optimized structures are listed in Table S.3 of the Supporting Information.

The relative energies for the four most competitive structures ((i) D_{2h}, (ii) C_{3v}, (iii) $C_{2h}(1)$, and (iv) $C_{2v}(1)$) are shown in Table 2. Structures (v) $C_{2v}(2)$, (vi) $C_{2v}(3)$, and (vii) D_{4h} (Figure 2) are significantly higher in energy than the D_{2h} and C_{3v} structures. For example, the $C_{2v}(2)$ structure (resulting from an end-on attack of a linear X−M−X on the M atom of its complement) is never competitive. Similarly, the $C_{2v}(3)$ structure is always at high energy, never a local minimum, and for all Be and Mg dihalides, it falls apart to two linear monomers during the optimization procedures. The quadruply bridged D_{4h} structure (vii), an intriguing possibility, also did not compete well. It was a local minimum only for the Sr and Ba dihalides. There it is +0.10 eV to +0.97 eV above the D_{2h} isomer, the best performance in the D_{4h} geometry coming from Ba_2F_4, at +0.10 eV.

The final three structures all collapse to one of the other structures. The doubly bridged in-plane cis $C_{2v}(4)$ and trans $C_{2h}(2)$ structures all optimize to the D_{2h} geometry. The C_s structure is also never a local minima, and the optimization product

(40) It is to be emphasized that the direct experimental bond distances have a different meaning from the computational minimum energy geometries (see ref 44) and that the latter have to be corrected for comparisons between theory and experiments to be valid. These corrections have typically not been performed in the old literature. See, e.g., Akishin P. A.; Spiridonov V. P. *Kristallografiya* **1957**, *2*, 475.
(41) *NIST-JANAF Thermochemical Tables. J. Phys. Chem. Ref. Data*; *Monograph No. 9*, 4th ed.; Chase, M. W., Ed.; 1998.
(42) (a) Ramondo, F.; Rossi, V.; Bencivenni, L. *Mol. Phys.* **1988**, *64*, 513. (b) Ramondo, F.; Bencivenni, L.; Cesaro, S. N.; Hilpert, K. *J. Mol. Struct.* **1989**, *192*, 83.
(43) Hargittai, M. Private communication. Varga, Z.; Lanza, G.; Minichino, C.; Hargittai, M. *Chem. Eur. J.*, in press.
(44) Hargittai, M.; Hargittai, I. *Int. J. Quantum Chem.* **1992**, *44*, 1057.
(45) Ramondo, F.; Bencivenni, L.; Spoliti, M. *THEOCHEM* **1992**, *277*, 171.
(46) Axten, J.; Trachtman, M.; Bock, C. W. *J. Phys. Chem.* **1994**, *98*, 7823.

Table 2. Relative Energies ($\Delta E = E$(isomer) $- E(D_{2h})$) Obtained at the B3LYP Computational Level for the More Competitive Dimer Geometries

	ΔE/eV[a]		
dimer	C_{3v}	$C_{2h}(1)$[b]	$C_{2v}(1)$[b]
Be_2F_4	1.70	D_{2h}	D_{2h}
Be_2Cl_4	1.24	D_{2h}	D_{2h}
Be_2Br_4	1.04	D_{2h}	D_{2h}
Be_2I_4	0.87	D_{2h}	D_{2h}
Mg_2F_4	0.72	D_{2h}	D_{2h}
Mg_2Cl_4	0.67	D_{2h}	D_{2h}
Mg_2Br_4	0.59	D_{2h}	D_{2h}
Mg_2I_4	0.54	D_{2h}	D_{2h}
Ca_2F_4	**−0.08**	D_{2h}	D_{2h}
Ca_2Cl_4	0.02	D_{2h}	D_{2h}
Ca_2Br_4	0.01	D_{2h}	D_{2h}
Ca_2I_4	0.02	D_{2h}	D_{2h}
Sr_2F_4	**−0.32**	−0.07	−0.03
Sr_2Cl_4	**−0.15**	D_{2h}	D_{2h}
Sr_2Br_4	**−0.12**	D_{2h}	D_{2h}
Sr_2I_4	**−0.11**	D_{2h}	D_{2h}
Ba_2F_4	**−0.54**	−0.32	−0.23
Ba_2Cl_4	**−0.32**	−0.07	−0.03
Ba_2Br_4	**−0.28**	−0.03	−0.01
Ba_2I_4	**−0.25**	−0.01	0.00

[a] Where the D_{2h} isomer is not the most stable isomer, ΔE for the most stable alternative is in bold type. [b] Most of the structures collapsed to a slightly distorted D_{2h} geometry ($\Delta E = 0.00$ eV).

appears to be quite sensitive to the details of the initial guess geometry. The structures optimized effectively to structure (i), (ii), or (iii) of Figure 2; see Table S.3. The optimized Be_2I_4 structure is a perturbed C_{3v} (C_s) geometry, which is marginally lower in energy compared to the C_{3v} structure (see footnote c in Table S.3 for details).

In Table 2, positive ΔE values indicate that the dimer is unstable in the specified geometry relative to the D_{2h} structure. A negative number indicates that that alternative geometry is more stable than the D_{2h} structure. For Be, Mg, Ca and most of the Sr dimers, the $C_{2h}(1)$ and $C_{2v}(1)$ geometries collapsed to an effective D_{2h} structure, with the terminal halides only very slightly (<1°) out of the plane of the four-membered ring.

The key results of Table 2 may be summarized as follows: The D_{2h} isomer is the most stable form for Be and Mg dihalides, as well as Ca_2Cl_4, Ca_2Br_4, and Ca_2I_4, while the C_{3v} structure is the most stable geometry for Ca_2F_4 and all the Sr and Ba dihalides.[47] The $C_{2h}(1)$ and $C_{2v}(1)$ variants, (see Figure 2) which could be described as trans and cis bent D_{2h} structures, compete only when the D_{2h} structure is unstable. And while they may be local minima, they are thermodynamically unstable with respect to C_{3v} geometries.

This conformational preference in the dimer structures may be correlated with the linear/bent structural variation in the monomers. The dimers of the bent monomers show the strongest preference for the C_{3v} arrangement (the most negative ΔE values in Table 2). In fact, the D_{2h} structure is only a transition structure for Ca_2F_4 and is a second-order saddle point for Sr_2F_4 and the Ba_2X_4 dimers (see Table S.3). On the other hand, the dimers of the Be and Mg monomers show the strongest preference for the D_{2h} arrangement (the more positive ΔE values in Table 2), with the C_{3v} structure being a second-order saddle point for Be_2X_4 (see Table S.3).

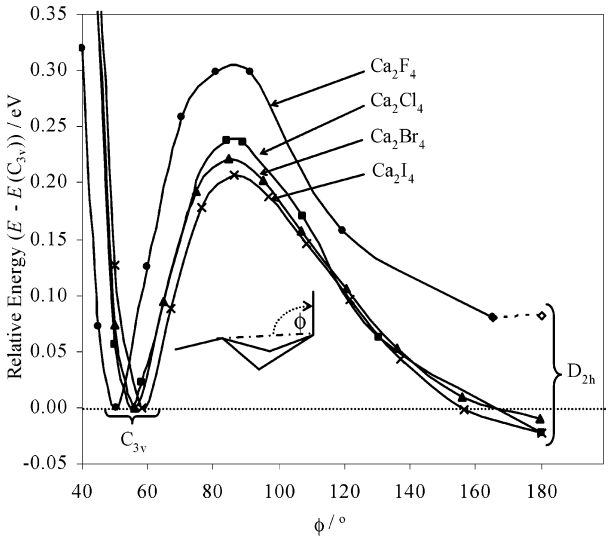

Figure 3. Optimized reaction path for the $C_{3v} \leftrightarrow D_{2h}$ rearrangements.

The structural linear/bent trend in the molecules does not perfectly match the D_{2h}/C_{3v} preferences in the dimers. For instance, all the Sr dimers show a preference for the C_{3v} geometry, even though the $SrBr_2$ and the SrI_2 monomers are not bent (see Table 1). The difference in energy of the D_{2h} and C_{3v} dimer structures ΔE is rather low, however: for Sr_2Br_4, $\Delta E = -0.12$ eV, and for Sr_2I_4, $\Delta E = -0.11$ eV (see Table 2).

As mentioned above, the CaF_2 dimer prefers the C_{3v} structure. The other three CaX_2 dimers show a preference for the D_{2h} geometry, but ΔE is pretty much insignificant for all of them ($\Delta E \approx 0.01$ eV to 0.02 eV) compared to the other dimers (Table 2, column 2). In fact, by far the most outstanding difference in the ΔE data computed at the B3LYP (Table 1) and the MP2 levels (Table S.4, column 2) is the reversal in structural preference of Ca_2Cl_4, Ca_2Br_4, and Ca_2I_4. At the MP2 level, the C_{3v} conformation is more stable than the D_{2h} one for these structures. However, the computed energy separations are again quite small, being less than 0.1 eV for all four Ca_2X_4 structures (Table S.4, column 2).

Interconversion of the Dimer Structures. We have talked about the difference in energy between the two prevalent dimer geometries, but actually how much does it cost to go from one form to the other? To answer this question we examined a linear transit between the C_{3v} and D_{2h} geometries for all four of the CaX_2 dimers using the transition structure optimization facility in Gaussian.[32,48] In each of these calculations, the starting (C_{3v} and D_{2h}) structures were slightly distorted to C_s symmetry by varying ϕ (Figure 3) by less than 1.0° from its value in the higher symmetry structures. During the optimization procedure, all the coordinates were allowed to vary.[49]

(47) Both geometries are local minima on the potential surfaces of Mg_2X_4, Ca_2Cl_4, Ca_2Br_4, Ca_2I_4, Sr_2Cl_4, Sr_2Br_4, and Sr_2I_4. For these systems, no imaginary frequency is obtained for either of the two isomers. For the beryllium dihalides, the C_{3v} isomer is not a local minimum. Conversely, for the Ca_2F_4, Sr_2F_4, and BaX_2 structures, the D_{2h} structure is not a local minimum (see Table S.3).

(48) Foresman, J. B.; Frisch, Æ. *Exploring Chemistry with Electronic Structure Methods*, 2nd ed.; Gaussian, Inc.; Pittsburgh, PA, 1995−96; Chapter 3, pp 46−49.

(49) Regions outside the direct transit between C_{3v} and D_{2h} in Figure 3 were not computed in the automatic reaction path optimization procedure. The portion of the curves in Figure 3 outside the transit between the C_{3v} and D_{2h} structures (to the left of the C_{3v} structures in the figure) were computed independently. The structures were optimized for fixed values of ϕ between 40° and $\phi(C_{3v})$.

The calculations were performed at the B3LYP level using the basis sets described in the Theoretical Methods section. For Ca_2F_4 and Ca_2Cl_4 the calculations were particularly expensive, since the cc-pVTZ all-electron basis sets were used for the F and Cl atoms, while core pseudopotentials were used for Br and I. For easier convergence, a guessed transition structure was also provided for the Ca_2F_4 and Ca_2Cl_4 transits calculations. Furthermore, only seven waypoint structures were optimized along the reaction path for these two dimers; for the heavier dihalides, 10 structures were optimized along the path (Figure 3). In Figure 3, the structural energies have been plotted as a function of ϕ, the angle formed between the two metal sites and the halide that rotates out of the triply bridged region in the "C_{3v}" structure (cf. structures (ii) and (x) in Figure 2) to become a terminal atom in the "D_{2h}" structure (cf. structures (i) and (ii) in Figure 2). Although all the parameters were optimized along the trajectory, ϕ is an ideal reaction coordinate for monitoring the $C_{3v} \leftrightarrow D_{2h}$ excursion, since it undergoes the most significant change overall, from between 50° and 60° to 180°.

Recall that for Ca_2Cl_4, Ca_2Br_4, and Ca_2I_4 both geometries are minima on the potential energy surface (Table 2). For these systems, the computed energy barriers are 0.24 eV, 0.22 eV, and 0.21 eV, respectively, for $C_{3v} \rightarrow D_{2h}$ isomerization (Figure 3), and they are only marginally larger (by 0.01−0.02 eV) for the reverse process ($D_{2h} \rightarrow C_{3v}$). The interconversion between the two isomers is "allowed"; there are no level crossings along this reaction path. Since the barriers between the C_{3v} and D_{2h} isomers are relatively low, and there is only a marginal difference in thermodynamic stability (ΔE in Table 2 is small), one might anticipate finding both isomers in the gas phase of Ca_2Cl_4, Ca_2Br_4, and Ca_2I_4. To the best of our knowledge, however, only the D_{2h} structure has been observed in matrix isolation studies.[42b,50] It would be interesting to effect a rapid quenching from the gas phase in a search for the possible C_{3v} structure.

In the case of Ca_2F_4, the kinetic barrier to the $C_{3v} \rightarrow D_{2h}$ isomerization is 0.30 eV, making the Ca_2F_4 C_{3v} structure the most kinetically stable of all the CaX_2 structures in that geometry (see Figure 3). The corresponding barriers for Ca_2Cl_4, Ca_2Br_4, and Ca_2I_4 (vide supra) are roughly 0.06 eV to 0.09 eV lower. Probably because the actual D_{2h} isomer is only a transition structure on the Ca_2F_4 potential energy surface, the automatic $D_{2h} \leftrightarrow C_{3v}$ structure optimization procedure gives a final product on the D_{2h} side in Figure 3 in which ϕ is noticeably smaller ($\phi \approx 165°$) than the ideal of 180° in the D_{2h} structure. We have added the data point for the D_{2h} structure from a separate optimization (unshaded box at the D_{2h} end of the Ca_2F_4 trajectory in Figure 3). The optimized D_{2h} and final transit structures are separated in energy by just 0.002 eV.

Pogrebnaya et al. have also computed the $C_{3v} \leftrightarrow D_{2h}$ transit for Ca_2F_4 at the MP2 level previously.[19] The barriers they obtained for both directions (~0.41 eV for $C_{3v} \rightarrow D_{2h}$ and 0.27 eV for $D_{2h} \rightarrow C_{3v}$) are ~0.1 and 0.05 eV, respectively, larger than the values we find at the B3LYP level (see Figure 3). The computed energy difference between the C_{3v} and D_{2h} structures in that work (0.10 eV)[19] is in reasonable agreement, however, with our computed result (0.08 eV; see ΔE for Ca_2F_4 in column 2 of Table 2).

To sum up, the group 2 dihalide dimers, M_2X_4, exhibit structural preferences that are correlated with the structural preferences in the MX_2 monomers. The relative thermodynamic stability of the D_{2h} and C_{3v} structures (see ΔE in Table 2) shows a direct correlation with the extent of the bending in and the flexibility of the monomers. The dimers of the molecules that are most bent (BaF_2, $BaCl_2$, $BaBr_2$, SrF_2) have the most stable C_{3v} structures (Table 2, column 2); the most rigid of the linear molecules (BeX_2 and MgX_2) show the strongest preference for the D_{2h} dimer conformation. The energy differences between the isomers are marginal for Ca_2X_4 X = Cl, Br, and I (Table 2).

It does not take much energy to interconvert the dimer structures; the barrier to ($C_{3v} \leftrightarrow D_{2h}$) interconversion is between 0.20 eV and 0.25 eV in either direction for all three systems. For Ca_2F_4, the C_{3v} structure is stable relative to the D_{2h} isomer and is, by all accounts, the global minimum on the potential surface (Table 2, Figure 3).

A Frontier Orbital Perspective on MX_2 Dimerization. The relationship of the monomer (MX_2) and dimer (M_2X_4) geometries is one of our points of interest. Perhaps another way into their similarities and differences is through a consideration of the dimerization process. Here qualitative frontier orbital considerations may be of value.

The basic idea of frontier orbital molecular orbital (MO) theory is that essential bonding interactions (leading to low kinetic barriers to reaction and thermodynamic stability; unfortunately not very clearly differentiated) will be those maximizing two-orbital two-electron bonding interactions and minimizing two-orbital four-electron antibonding interactions. The maximization or minimization is governed by the perturbation theory expressions for the interaction of two orbitals of energies E_i° and E_j°

$$\Delta E = \frac{|H_{ij}|^2}{E_i^\circ - E_j^\circ}$$

with the Hamiltonian H_{ij} roughly proportional to $-S_{ij}$, the negative of the overlap integral.

Many interactions are governed by acid−base interactions (interactions of an acceptor orbital on one component with a donor orbital on the other). Let us trace the consequences of such a perspective for the MX_2 dimerization. We begin with the important valence orbitals (the highest occupied and lowest unoccupied MOs) of a linear and bent MX_2 molecule illustrated in Figure 4.

The diagram is just an approximate representation of the valence orbitals of the group 2 dihalides; we should keep in mind that the contribution of the M and X sites to the orbitals will vary significantly going from Be to Ba and from F to I. As the electronegativity difference between M and X increases, the frontier MOs will be increasingly dominated by the halide contributions. M. Hargittai has pointed out, for instance, that a look at the frontier orbitals of $SrCl_2$, far more ionic than the Be and Mg analogues, reveals that the participation of the Sr site is insignificant.[43]

The unusual coefficient pattern in the allylic π orbitals in Figure 4 is due to the relative electronegativity of M and X.

(50) Vajda, E.; Hargittai, M.; Hargittai, I.; Tremmel, J.; Brunvoll, J. *Inorg. Chem.* **1987**, *26*, 1171.

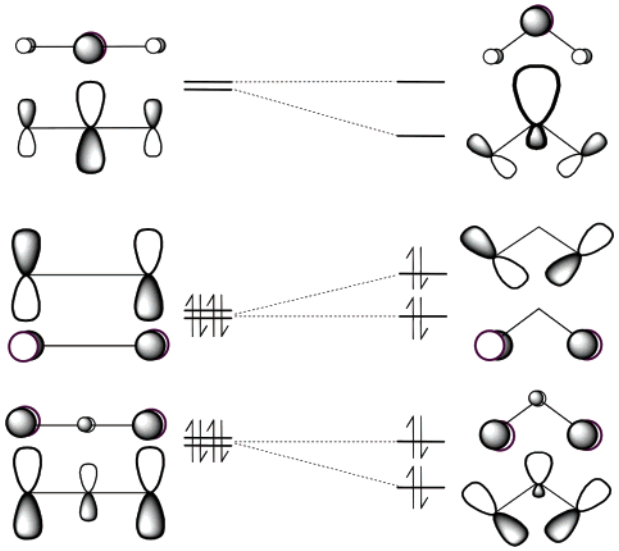

Figure 4. Representations of the highest occupied MOs (HOMOs) and lowest occupied MOs (LUMOs) in the linear and bent group 2 metal dihalide.

The only essential change on bending is the formation of an "out-pointing" hybrid at M in the LUMO. The high lying donor orbitals are halide *p*-type lone pair combinations (in and out of plane, with some central M *np* admixture in some orbitals). The acceptor orbitals are *np*'s localized on M (with important *ns* hybridization, if bent, as well as some antibonding X lone pair admixture).

The eventual equilibrium dimer geometries are the outcome of optimizing all interactions; perhaps the frontier orbital perspective is most useful in thinking about the early stages of dimerization. Geometries of approach such as (A) in Figure 5 have one good HOMO−LUMO interaction. Geometries such as (B) in Figure 5 symmetrize the situation, leading to two reinforcing frontier orbital interactions. In (C), a bending at M helps the dimer achieve two stabilizing fragment molecular orbital (FMO) interactions.

It is not a far stretch of the imagination to envisage the symmetrization of structures (B) and (C) to the competitive D_{2h} and C_{3v} dimer structures. And, just to be fair, we are led to think of approaches (B) and (C) by knowing the product dimer geometries.

We believe that the frontier MO viewpoint provides us with a perspective on how monomer geometries might be related to preferred dimer (or polymer) geometry. If frontier MO interactions are not optimized in an initial dimer geometry, perhaps they might be optimized better if the monomer fragments are allowed to distort (bend). We do not intend to turn this into a quantitative estimate; it is just a way of thinking. Nonetheless, one is led to another question. What are the energy scales of bending (or linearization) vs dimerization? We explore this in the next section.

Dimer−Monomer Relationship

First, let us look in some detail at the geometry of the dimer. The optimized (B3LYP) geometric parameters of the lowest energy (D_{2h} or C_{3v}) structure of each dimer are given in Table 3. The corresponding MP2 geometries have been computed, as well, and are summarized in Table S.4 of the Supporting Information. The two sets of computational data show very good qualitative agreement. So, for the rest of our discussion we will focus on the DFT (B3LYP) values in Table 3. The vibrational frequencies obtained at the B3LYP level for all the D_{2h} and C_{3v} dimer structures are included in the Supporting Information as well (Table S.5a,b).

The linear conformation exhibited in the gas phase by some of the dihalides is, of course, lost in the dimers. The D_{2h} structures (see Table 3) may be viewed as an in-plane combination of two monomers each with bond angle α. This angle is in the range $128° < \alpha < 138°$ for all the stable D_{2h} structures, and the bridging M−X bonds are almost always ∼0.2 Å longer than the terminal M−X bonds (Table 3). In the C_{3v} structures (see Table 3), the bond angle β between the terminal halide and the bridging halides is similar in magnitude to α in the D_{2h} structures: $128° < \beta < 138°$. Within the triply bridged region of the minimum energy C_{3v} structures, the bond angle γ is, of course, significantly smaller. In Table 3, $79° < \gamma < 92°$, decreasing as M gets larger and X gets smaller.

The need for very small γ angles in the optimized C_{3v} conformation provokes the speculation that this dimer conformation should be disfavored for Be, Mg, and most of the Ca dimers, for the same reasons that a bent geometry is disfavored in their monomers. Similarly, we might speculate the C_{3v} conformation is favored in Ca_2F_4, Sr_2X_4, and Ba_2X_4 for the same reason the bent monomer geometry is favored.

But let us examine this argument in greater detail. To do so, two key quantities will be considered. The monomer "preparation" or "deformation" energy E_{def} is defined as the energy cost of preparing the optimized monomer for dimer formation by changing the bond lengths and angle to those of the MX_2 fragments within the D_{2h} and C_{3v} dimers. The relevant fragments are illustrated in Figure 6.

In the D_{2h} isomer, both fragments are identical with M−X bonds of length *a* and *b* and bond angle α. In the C_{3v} isomer, one fragment has M−X distances *c* and *d* and bond angle β, while the other fragment has equal M−X bonds of length *e* and bond angle γ. The total deformation energies for the MX_2 fragments of the D_{2h} and C_{3v} structures, $E_{def}(D_{2h})$ and $E_{def}(C_{3v})$, are listed in Table 4. The E_{def} values for the individual fragments are given in Table S.6.

Also included in Table 4 are the counterpoise corrected dimerization energies E_{dim} that have been computed for both the C_{3v} and D_{2h} isomers: $E_{dim} = E^{CP}(M_2X_4) - 2E(MX_2)$. In each case (monomer and dimer), of course, the respective minimum energy geometries were used. $E^{CP}(M_2X_4)$ was obtained by adding the counterpoise correction[51] δ^{CP} to the energy $E(M_2X_4)$ of the optimized dimer structure to correct approximately for basis set superposition errors (BSSE). $E(MX_2)$ is the energy of the optimized monomer.

MX_2 Deformation Energies. Let us look first at the dependence of the D_{2h} and C_{3v} deformation energies (columns 3 and 4 of Table 4) on the atomic number of M and X. All the deformation energies are, of course, positive; in each case we are going from the absolute minimum to some higher energy structure on the monomer potential energy surface. For each metal atom, E_{def} changes in the order F > Cl > Br > I for both isomers. While this result is simple, the pattern is not easy to

(51) The counterpoise correction δ^{CP}, and $E^{CP}(M_2X_4)$, were obtained directly from our Gaussian 03 calculations. The definition of δ^{CP} and steps involved in calculating it are outlined in: Jensen, F. *Introduction to Computational Chemistry*, Wiley: New York, 1999; pp 172−173.

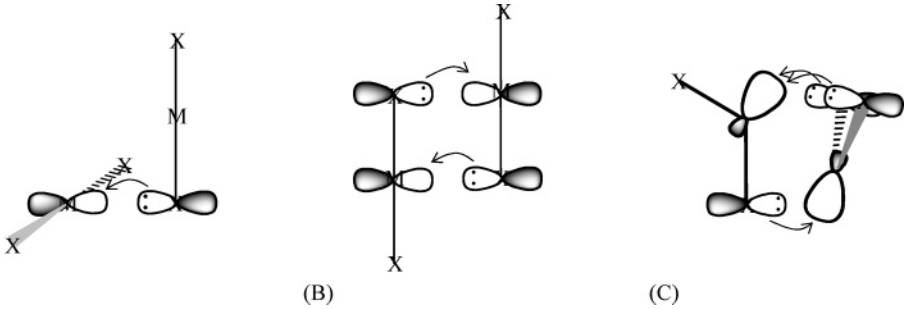

Figure 5. Possible interactions leading to D_{2h} and C_{3v} dimer formation.

Table 3. Optimized (B3LYP) Geometries for the D_{2h} and C_{3v} Isomers of the Group 2 Dihalide Dimers[a]

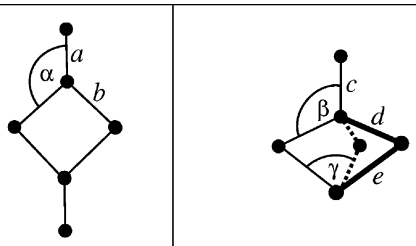

Dimer	*a*	*b*	α	*c*	*d*	*e*	β	γ
Be_2F_4	1.382	1.566	134.4	*1.381*	*1.787*	*1.498*	*131.8*	*100.7*
Be_2Cl_4	1.827	2.006	129.9	*1.824*	*2.265*	*1.936*	*127.4*	*107.3*
Be_2Br_4	1.994	2.176	129.3	*1.991*	*2.446*	*2.102*	*126.1*	*109.0*
Be_2I_4	2.213	2.388	128.5	*2.211*	*2.669*	*2.309*	*124.5*	*111.2*
Mg_2F_4	1.762	1.914	139.0	*1.772*	*2.056*	*1.860*	*133.0*	*88.9*
Mg_2Cl_4	2.192	2.374	133.6	*2.203*	*2.570*	*2.307*	*128.9*	*97.3*
Mg_2Br_4	2.354	2.543	132.8	*2.364*	*2.755*	*2.473*	*127.9*	*99.2*
Mg_2I_4	2.566	2.764	131.1	*2.575*	*2.993*	*2.685*	*126.4*	*102.0*
Ca_2F_4	*1.996*	*2.187*	*141.0*	2.008	2.302	2.087	135.8	83.6
Ca_2Cl_4	2.452	2.664	136.5	*2.465*	*2.803*	*2.562*	*131.4*	*90.6*
Ca_2Br_4	2.625	2.834	136.0	*2.638*	*2.979*	*2.738*	*130.3*	*91.8*
Ca_2I_4	2.845	3.057	134.1	*2.860*	*3.212*	*2.960*	*128.6*	*94.5*
Sr_2F_4	*2.152*	*2.347*	*142.0*	2.167	2.455	2.235	136.9	81.1
Sr_2Cl_4	*2.622*	*2.837*	*137.9*	2.639	2.964	2.722	132.7	87.8
Sr_2Br_4	*2.802*	*3.013*	*137.6*	2.817	3.148	2.908	131.7	88.8
Sr_2I_4	*3.025*	*3.241*	*135.6*	3.040	3.383	3.135	129.9	91.7
Ba_2F_4	*2.295*	*2.519*	*142.4*	2.310	2.631	2.388	138.4	78.7
Ba_2Cl_4	*2.791*	*3.027*	*139.0*	2.810	3.146	2.894	134.2	84.9
Ba_2Br_4	*2.985*	*3.207*	*139.1*	3.001	3.332	3.089	133.5	85.4
Ba_2I_4	*3.212*	*3.441*	*137.2*	3.230	3.571	3.323	131.5	88.3

[a] See the Theoretical Methods section for the basis sets used. The geometries for the higher energy dimer structure are in italics.

explain. Deformation involves a *decrease* in the $X\overset{e}{-}M\overset{e}{-}X$ bond angle in instances where the monomer bond angle, Θ, is larger than the angles in dimer fragments. However, an *increase* in the bond angle is necessary when the monomer is bent already (e.g., BaF_2), so that Θ is smaller than α or β. Furthermore, bond length changes required in going from the monomer to the prepared fragment, such as the stretching of the monomer bond to match *b* and *d* (cf. Table 1 and Table 3), must also be considered.

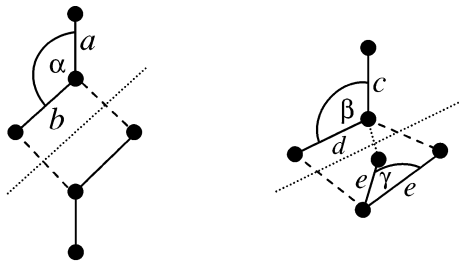

Figure 6. Illustration of MX_2 monomer fragments for which the deformation energies E_{def} have been computed (see Table 4): (a) the $X\overset{a}{-}M\overset{b}{-}X$ fragment, bond angle = α, in the D_{2h} structure, and (b) $X\overset{c}{-}M\overset{d}{-}X$, bond angle = β and $X\overset{e}{-}M\overset{e}{-}X$, bond angle = γ in the C_{3v} structure.

For the $X\overset{e}{-}M\overset{e}{-}X$ fragment in C_{3v} structure, γ is always smaller than Θ. So it is easier to identify relationships between the deformation energies of this fragment and the extent of the angle and distance changes required to prepare the monomer fragments for bonding. We observe, in fact, that E_{def} for this fragment (column 6 in Table S.6) varies indirectly with γ; that is, the structures with the smallest bond angles require the largest deformation energies.

We mentioned in our initial discussion of the monomers (vide supra) that as M gets larger and softer, bending of the MX_2 monomer becomes less expensive and even pays off for the larger cations.[26] We have therefore not been surprised by a general decrease in the value of $E_{def}(C_{3v})$ going from M = Be to M = Ba (column 4, Table 4), since the preparation of the $X\overset{e}{-}M\overset{e}{-}X$ fragment in particular always involves significant bending. A decrease in the deformation energy as M gets larger is observed in $E_{def}(D_{2h})$ as well. As mentioned above, the computed energies for the D_{2h} structures of the heavier metal atoms with bent monomers are more difficult to interpret. Nonetheless, the decrease in the energy cost of preparing the D_{2h} fragment (whether by reducing or enlarging the monomer bond angle) is consistent with the view that the softer the metal atom is, the easier it is for any deformation of the structure (in bond length or bond angle) to occur.

Next we have to consider the differences in the magnitude of $E_{def}(C_{3v})$ and $E_{def}(D_{2h})$ and the possible implications for geometric preferences in the dimer. First, the deformation energies E_{def} (Table 4) for the D_{2h} structure are always lower than the deformation energies for the C_{3v} structures. This is the case even where the C_{3v} structure is the more stable isomer! For instance, although the BaF_2 C_{3v} dimer is more stable (by 0.54 eV; Table 2), the energy cost to prepare the MX_2 C_{3v} dimer fragments ($E_{def}(C_{3v})$ = 1.24 eV; Table 4) is nearly twice the

Table 4. Computed Energies for the Rearrangement (Deformation) of Pairs of Stable MX_2 Monomers to the Conformations Observed in the (D_{2h} and C_{3v}) M_2X_4 Dimers E_{def},[a] and the Counterpoise Corrected Dimerization Energies $E_{dim} = (E^{CP}(M_2X_4) - 2 \times E(MX_2))$[b,c]

preferred isomer		E_{def}/eV		E_{dim}/eV	
		$E_{def}(D_{2h})$	$E_{def}(C_{3v})$	$E_{dim}(D_{2h})$	$E_{dim}(C_{3v})$
Be_2F_4	D_{2h}	**1.87**	4.15	**−1.26**	0.49
Be_2Cl_4	D_{2h}	**1.72**	3.24	**−0.73**	0.53
Be_2Br_4	D_{2h}	**1.56**	2.85	**−0.60**	0.47
Be_2I_4	D_{2h}	**1.44**	2.54	**−0.45**	0.45
Mg_2F_4	D_{2h}	**0.94**	2.76	**−2.43**	−1.67
Mg_2Cl_4	D_{2h}	**1.02**	2.28	**−1.48**	−0.78
Mg_2Br_4	D_{2h}	**0.96**	2.05	**−1.23**	−0.64
Mg_2I_4	D_{2h}	**0.93**	1.86	**−1.00**	−0.44
Ca_2F_4	C_{3v}	0.43	**1.44**	−2.60	**−2.62**
Ca_2Cl_4	D_{2h}	**0.43**	1.21	**−1.97**	−1.92
Ca_2Br_4	D_{2h}	**0.40**	1.09	**−1.80**	−1.75
Ca_2I_4	D_{2h}	**0.41**	1.01	**−1.59**	−1.53
Sr_2F_4	C_{3v}	0.46	**1.26**	−2.40	**−2.69**
Sr_2Cl_4	C_{3v}	0.30	**0.96**	−2.02	**−2.14**
Sr_2Br_4	C_{3v}	0.28	**0.89**	−1.86	**−1.96**
Sr_2I_4	C_{3v}	0.30	**0.83**	−1.66	**−1.74**
Ba_2F_4	C_{3v}	0.69	**1.24**	−1.87	**−2.43**
Ba_2Cl_4	C_{3v}	0.34	**0.83**	−1.81	**−2.10**
Ba_2Br_4	C_{3v}	0.23	**0.69**	−1.78	**−2.03**
Ba_2I_4	C_{3v}	0.21	**0.60**	−1.64	**−1.91**

[a] $E_{def}(D_{2h}) = 2[E(X^{a}M^{b}X; \angle = \alpha) - E(X^{r}M^{r}X; \angle = \Theta)]$ for the D_{2h} structure. Similarly, $E_{def}(C_{3v}) = [E(X^{c}M^{d}X; \angle = \beta) + E(X^{e}M^{e}X; \angle = \gamma)] - 2E(X^{r}M^{r}X; \angle = \Theta)$ for the C_{3v} structure (see Figure 6); $\angle \equiv$ bond angle. [b] The correction for basis set superposition errors has been accomplished by the addition of a counterpoise correction to the computed energy $E(M_2X_4)$, so $E^{CP}(M_2X_4) = E(M_2X_4) + \delta^{CP}$. The counterpoise correction, δ^{CP}, and $E(M_2X_4)$ were obtained at the same computational level (see Theoretical Methods section). [c] The values of E_{def} and E_{dim} for the preferred structures are in bold type.

cost of preparing the MX_2 fragments of the D_{2h} dimer ($E_{def}(D_{2h}) = 0.69$ eV; Table 4). The variation in the deformation energies, therefore, does not by itself explain the D_{2h}/C_{3v} structural preferences in the dimers.

Dimerization Energies and Structural Preferences. The outcome of a destabilization in preparing the MX_2 monomer for its geometry in the dimer plus the stabilization upon dimerization is the dimerization energy (E_{dim}: columns 5 and 6 of Table 4). This quantity is generally negative for both the D_{2h} and C_{3v} dimers, indicating that the dimer is stable relative to monomers. Only for the beryllium dimers in the C_{3v} geometry are the dimerization energies positive; $E_{dim} \approx +0.5$ eV in each case! Dimerization in the strained C_{3v} geometry does not in the end pay off for the beryllium dihalides. For all the other systems, both the D_{2h} and C_{3v} dimers are stable relative to the monomers, with the more stable of the two dimers having the more negative dimerization energy (values in bold in columns 5 and 6 of Table 4).

A comparison of the dimerization energies and the deformation energies in Table 4 enables us to rationalize the structural preferences in the dimer and to better understand the link to the bending in the monomer. The strong preference for the D_{2h} structure in the beryllium dimers is explained by the quite large deformation energies needed to prepare the BeX_2 C_{3v} fragments compared to the deformation energies for the BeX_2 D_{2h} fragments (Table 4). The stabilization during the formation of the Be_2X_4 C_{3v} dimer is too small to compensate for the large deformation energy.

For the magnesium dihalides, the deformation energies are smaller than they are for the beryllium dihalides, and the stabilization upon dimerization is large enough for both the D_{2h} and C_{3v} isomers to be stable relative to the monomers (E_{dim} negative for both isomers). Nonetheless, the D_{2h} isomer, which has the smaller deformation energy, is more stable than the C_{3v} form.

The geometric preferences in the beryllium and magnesium dimers are explained by the large deformation energies and weak stabilization of the C_{3v} structure. But how to explain the emergence of a preference for the C_{3v} structure as M gets larger? As mentioned previously, $E_{def}(C_{3v})$ is larger than $E_{def}(D_{2h})$ for all the dimers. However, both $E_{def}(C_{3v})$ and $E_{def}(D_{2h})$ decrease going from Be to Ba, and this is accompanied by a significant stabilization of the C_{3v} isomers relative to the D_{2h} isomer.

This stabilization is evident from the sharp reduction in the gap between the D_{2h} and C_{3v} dimerization energies as M gets larger. For instance, the difference between $E_{dim}(C_{3v})$ and $E_{dim}(D_{2h})$ for BeF_2, MgF_2, and CaF_2 is 1.75 eV, 0.76 eV, and −0.02 eV, respectively (see columns 5 and 6 of Table 4), the negative sign on the last number indicating that the CaF_2 C_{3v} isomer is more stable than the D_{2h} isomer. Dramatic reductions in $E_{dim}(C_{3v}) - E_{dim}(D_{2h})$ are observed going from BeX_2 to CaX_2 (X = Cl, Br, and I) as well. We have pointed out already, in fact, that the D_{2h} structures of Ca_2Cl_4, Ca_2Br_4, and Ca_2I_4 are not separated from their C_{3v} isomers by much.

For the larger (Sr and Ba) metals, the C_{3v} structures win out ($E_{dim}(C_{3v}) < E_{dim}(D_{2h})$) for all the dimers. Even though the strontium bromide and iodide monomers are linear, the stabilization on forming the C_{3v} structure is enough to compensate for the cost of the significant bending and bond length variations that are necessary to stabilize the C_{3v} isomer relative to the D_{2h} structure.

To sum up this section, the deformation energies, E_{def}, play a decisive role in dimer formation and are responsible in large part for the strong preference for the D_{2h} structure in Be_2X_4 and Mg_2X_4. This interpretation is in line with the strong preference in the BeX_2 and MgX_2 monomers for a linear geometry. E_{def} loses significance for the larger cations, however. To begin with, some of the heavier dihalides are already quite bent, and for the floppy (bent and linear) molecules dimerization in the C_{3v} geometry is typically more feasible, as it allows better orbital overlap and interactions leading to bond formation at only a small cost.

A complete correspondence between linear(bent) monomer and $D_{2h}(C_{3v})$ dimer structural preferences is not observed, however. The linear $SrBr_2$ and SrI_2 monomers, for example, show a relatively weak preference for the C_{3v} geometry. A simple connection between the monomer and dimer structural preferences can be made nonetheless, if we make reasonable allowances for the more floppy monomers.

Interactions Influencing MX_2 Dimerization. As mentioned previously, the bending in the monomers is enhanced by both the involvement of *d* orbitals in the bonding and the polarization of the cationic core by the halide anions.[2,26] We suggest that these influences are of key importance in explaining the dimer structures as well.

In the C_{3v} structures, the availability of sd^x hybrid orbitals makes it possible for the metal ions to form the three equivalent polar bonds in the bridge region of the C_{3v} dimer at relatively

small (<90°) X−M−X angles, an undertaking that would likely be more expensive if only sp^x hybrid orbitals were available. In the Be and Mg systems, the reverse is true. *d* orbitals are unavailable, and the cation is sp^x hybridized.

The structural variation in the dimers has been rationalized from a purely electrostatic viewpoint, also. Gigli et al. have applied a classical polarized-ion model to the (Mg to Ba) dihalide dimers,[17,18] suggesting in 1977[17] that "...polarization effects, mainly the charge-dipole interactions,...may play a similar role in the polymerization process." as they do in the molecule. They predicted, by an electrostatic model, that the D_{2h} dimer conformation was the minimum energy arrangement (compared to (ii), (iii), (iv), and (vi) in Figure 2) when the cation polarizability is small, as in the Mg_2X_4 systems.[17,18] They also succeeded in demonstrating the relative stability of the C_{3v} conformation (ii) and structures (iii) and (iv) (Figure 2) compared to the D_{2h} conformation for dimers with the larger cations and smaller anions.[18]

The structural preferences in the dimers were explained by the polarizability dependence of the dimer formation energy. The small X−M−X angles in the C_{3v} structures are stabilized by charge−dipole and dipole−dipole interactions between the M and X sites. The strength of these interactions varies directly with the size of the dipoles induced at M, so the stability of the C_{3v} structure is dependent on the polarizability of M and the charge on the halide sites: the larger the cation polarizability, and the larger the charge separation along the MX bond (the more electronegative X is), the more stable the C_{3v} structure will be. In the systems where the cation is small and not very polarizable, the X- - -X repulsive interactions predominate and the D_{2h} structure (with two halides, rather than three, in the bridge region) is the preferred conformation.

To sumarize, it is evident that (aside from the energetics of dimerization) the D_{2h}/C_{3v} structural preferences in the M_2X_4 systems may be explained qualitatively using a language already familiar to us from earlier work on the linear/bent structural variations in the MX_2 monomers. The preferences in both the monomers and the dimer are explained by the same electronic and electrostatic influences: the availability of *d* orbitals at M for mixing with the *s* and *p* orbitals and core-polarization effects.

MX_2 Crystal Structures

Next we turn our attention to the extended MX_2 crystal structures; these are, of course, the familiar (and thermodynamically stable) forms in which these compounds commonly occur under ambient terrestrial conditions. We start off with a question. To what extent do the interactions that determine the structure of a molecule influence structural preferences in the extended solid? Put another way, does a solid remember the monomer? The question is asked where it is of interest, of course; for molecular crystals we know the answer: "very well". We want a more challenging system, and crystals thought to be largely ionic certainly offer us that. Specifically, we want to examine the preferences in the extended solid-state structures of the group 2 dihalides. These proclivities will be considered in the broader context of the structural preferences in the group 2 dihalide monomers and dimers, which have been considered in preceding sections.

A relevant observation was made by M. Hargittai and Jancsó,[52] who pointed out that dimers were observed in the vapors of various main group and transition metal dihalides only when dimer fragments were identifiable in the corresponding solid. Additionally, the heat of vaporization of the dimer had to be no more than about 0.43 eV (10 kcal/mol) larger than that of the monomer.

The perceptive remarks by Kaupp at the end of his 2001 review of "non-VSEPR" structures[2] are also noteworthy. In that work, he suggested that the factors responsible for the unexpected geometries of the alkaline earth MX_2 and other compounds may account for unusual structural preferences—specifically, unsymmetrical coordination—in their extended solids as well. He surmised, for example, that the unsymmetrical coordination in the extended solids of some of the heavy alkaline earth dihydrides and dihalides with the $PbCl_2$ structure type is likely due to the involvement of *d* orbitals in the bonding and to core polarization. So far, however, a relationship between structural preferences in the gas phase and in the solid phases of the group 2 dihalides has not been examined systematically.

The structure types exhibited by the group 2 dihalides at ambient conditions[23,24,53−56] are summarized in Figure 7. Some of these are well-known: the SiO_2 (β-cristobalite) structure, the rutile (TiO_2) and the fluorite (CaF_2) structures. Some of the structure types may be less familiar, such as the $SrBr_2$ and the SrI_2 structures.

It will become important in drawing a connection to monomer and dimer structures to focus on the coordination environment of the metal atom (see Table 5). The BeX_2 crystals exhibit the diamond-type open structure of the SiO_2 β-cristobalite structure (ref 24b, pp 352, 787) and (SiS_2 type) chains[57] with tetrahedrally coordinated Be centers (see Table 5 and Figure 7a,b). In both structures the coordination number, CN, at the metal sites is 4. The magnesium dihalides and the $CaCl_2$, $CaBr_2$, and CaI_2 crystals span a range of structure types, all with six-coordinate metal sites: the TiO_2 (rutile) and $CaCl_2$ types are stacks of edge-sharing octahedra,[58] while the $CdCl_2$ and CdI_2 types are layer structures, with edge-sharing octahedra within each layer (see Figure 7; ref 24).

The remaining structures represent roughly three different structure types. SrI_2 has a unique seven-coordinate metal center (Figure 7g),[54] while the others adopt either the 7 + 2 $PbCl_2$ structure type or the eight-coordinate fluorite structure (see Figure 7h,i, and Table 5).[56] Note that $SrBr_2$ is sometimes classified simply as having the $PbCl_2$ structure type (e.g., ref 23, p 2911) but is probably better described as a significantly distorted $PbCl_2$ structure (ref 24b, p 378; ref 53). More recently, the structure has been described by Smeggil and Eick as a hybrid of the $SrCl_2$ and SrI_2 structures. Based on their single crystal

(52) Hargittai, M.; Jancsó, G. Z. *Naturforsch.* **1993**, *48*, 1000.
(53) Kamermans, M. A. *Z. Kristallogr*. **1939**, *101*, 406.
(54) Rietschel, V. E. Th.; Bärnighausen, H. *Z. Anorg. Allg. Chem.* **1969**, *368*, 62.
(55) Smeggil, J. G.; Eick, H. A. *Inorg. Chem.* **1971**, *10*, 1458. The crystal structure of $SrBr_2$ was found to be consistent with the *P*4/*n* space group.
(56) Pies, W.; Weiss, A. In Crystal Structure Data of Inorganic Compounds − Part a: Key Elements F, Cl, Br, I (VII Main Group) Halides and Complex Halides); Hellwege, K.-H., Hellwege, A. M., Eds.; Landolt-Börnstein New Series III, Vol. 7; Springer: Berlin, 1973.
(57) Troyanov, S. I. *Russ. J. Inorg. Chem.* **2000**, *45*, 1481; *Zh. Neorg. Khim.* **2000**, *45*, 1619.
(58) The TiO_2 (rutile) and $CaCl_2$ structures are homeotypic; TiO_2 is tetragonal (space group $P4_2/mnm$), while $CaCl_2$ is orthorhombic (space group *Pnnm*).

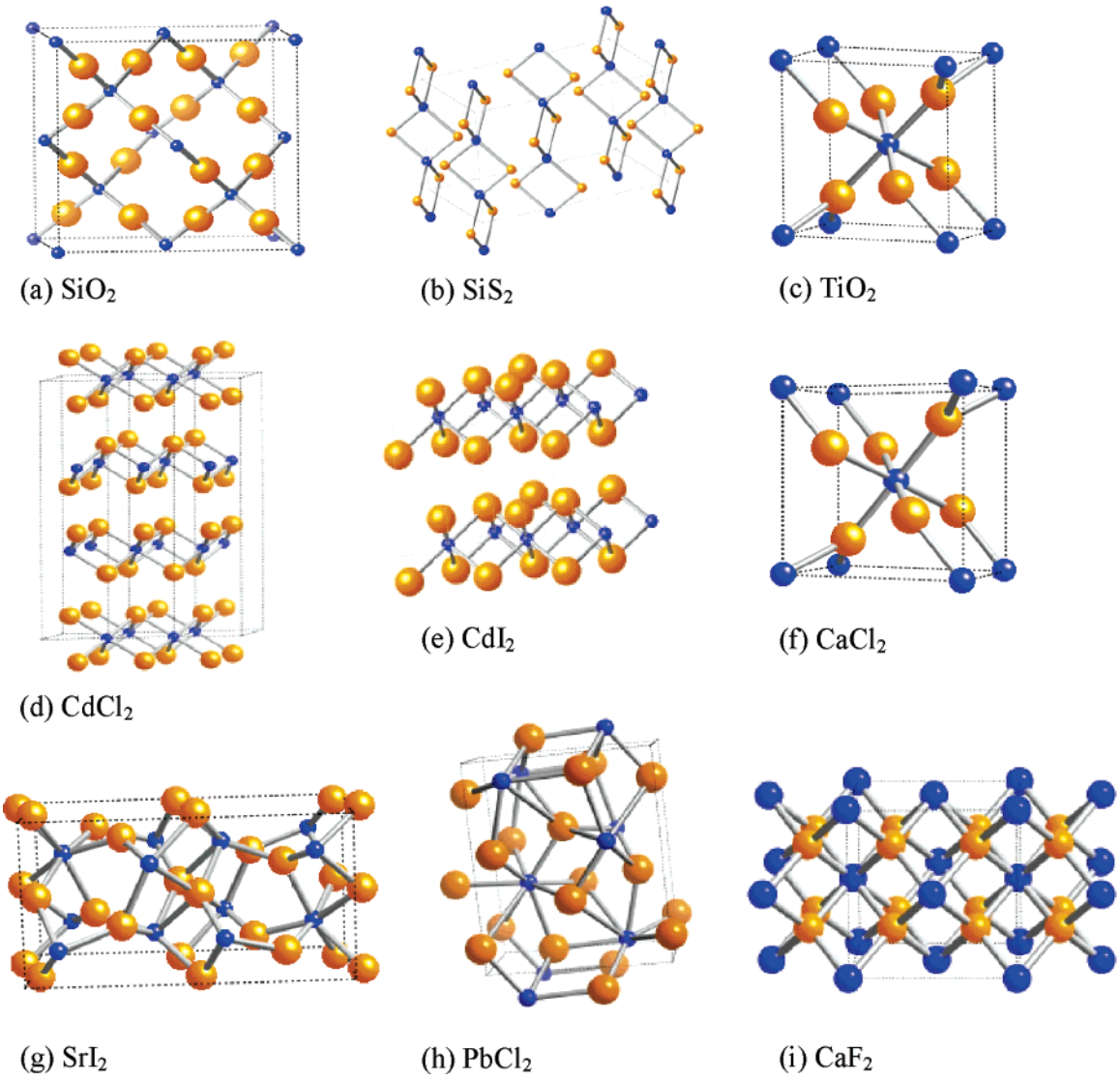

Figure 7. Structure types of the group 2 metal dihalide crystals.

Table 5. Structure Types and Metal Coordination Numbers (CNs) for Group 2 Dihalide Extended Solids at Ambient Conditions

crystal	type	CN
BeF_2	SiO_2	4
$BeCl_2$, $BeBr_2$, BeI_2,	SiS_2	4
MgF_2	TiO_2	6
$MgCl_2$	$CdCl_2$	6
$MgBr_2$, MgI_2, CaI_2	CdI_2	6
$CaCl_2$, $CaBr_2$	$CaCl_2$	6
SrI_2[a]	SrI_2	7
$SrBr_2$,[b] $BaBr_2$, BaI_2	$PbCl_2$	7 + 2
CaF_2, SrF_2, $SrCl_2$, BaF_2, $BaCl_2$[c]	CaF_2	8

[a] Unique structure; see Figure 7.[54] [b] $SrBr_2$ has been described as a distorted $PbCl_2$[24b,53] and, more recently, as a hybrid of the $SrCl_2$ (fluorite) and SrI_2 structures with seven- and eight-coordinate Sr sites.[55] [c] A $PbCl_2$ modification of $BaCl_2$ has been observed at ambient conditions, as well.[56,59] Note that both the fluorite (CaF_2) (CN = 8) and the $PbCl_2$ (CN = 7 + 2) modifications are high coordination structure types.

X-ray diffraction data, the Sr atoms are seven- and eight-coordinate, while the Br atoms are trigonally and tetrahedrally coordinated.[55] In the following sections $SrBr_2$ will be grouped with the regular $PbCl_2$, since the coordination number at Sr in $SrBr_2$ (CN = 7 and 8) coincide with the 7 + 2 coordination in the $PbCl_2$ structures.

Table 6 presents an overview of the structural preferences in the MX_2 monomers (bent or linear), the dimers (D_{2h} or C_{3v}), and the extended solid structures. A simple color coding system has been employed, which distinguishes the fluorite type and lead chloride structure types from the others. The basis for this partitioning will be clarified below.

In preparation for our analysis of the relationship between the molecular (monomer and dimer) structures and the solids, the smallest X−M−X angles (separation between nearest neighbor X sites bonded to the same cation) in each of the nine crystal structures (Figure 7) were examined. The average of these "nearest neighbor" X−M−X angles in the crystal structures are summarized in Figure 8. The bars in the figure have been arranged according to the size of the metal and halide atoms, giving priority to the smallest (lowest atomic number) atoms. The series runs, therefore, from the crystal structures of the Be dihalides (SiO_2 and SiS_2 types), through the (rutile, $CdCl_2$ and CdI_2) magnesium dihalides to the higher coordination structures. Additionally, the lower coordination solids are given priority, so that CaF_2, which is eight-coordinate, is plotted last. It has been difficult to determine where to position $PbCl_2$. The M site in that structure is best described as (7 + 2)-coordinate

Table 6. Structural Preferences in the Group 2 Dihalide Gas Phase Monomers and Dimers, and Extended Solids at Ambient Conditions[a]

		Be	Mg	Ca	Sr	Ba
F	*Mol. Structure*	Linear	Linear	Bent	Bent	Bent
	Dimer Structure	D_{2h}	D_{2h}	C_{3v}	C_{3v}	C_{3v}
	Structure type	***SiO_2***	***TiO_2***	***CaF_2***	***CaF_2***	***CaF_2***
Cl	*Mol. Structure*	Linear	Linear	Linear	Bent	Bent
	Dimer Structure	D_{2h}	D_{2h}	D_{2h}	C_{3v}	C_{3v}
	Structure type	***SiS_2***	***$CdCl_2$***	***$CaCl_2$***	***CaF_2***	***CaF_2*** [b]
Br	*Mol. Structure*	Linear	Linear	Linear	q-linear	Bent
	Dimer Structure	D_{2h}	D_{2h}	D_{2h}	C_{3v}	C_{3v}
	Structure type	***SiS_2***	***CdI_2***	***$CaCl_2$***	***$SrBr_2$*** [c]	***$PbCl_2$***
I	*Mol. Structure*	Linear	Linear	Linear	Linear	Bent
	Dimer Structure	D_{2h}	D_{2h}	D_{2h}	C_{3v}	C_{3v}
	Structure type	***SiS_2***	***CdI_2***	***CdI_2***	***SrI_2*** [d]	***$PbCl_2$***

[a] Coordination numbers at M in the extended solids are listed in Table 5. [b] See footnote c in Table 5. [c] See footnote b in Table 5. [d] See Figure 7g.

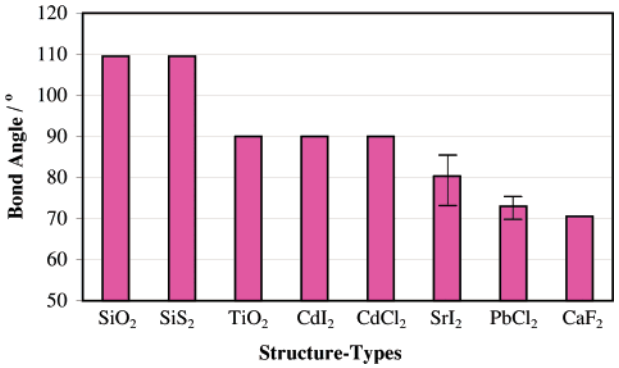

Figure 8. X−M−X angles between nearest neighbor X- - -X sites in the MX_2 structure types adopted by the group 2 metal dihalide crystals. The associated coordination numbers and MX_2 solids are listed in Table 5.

rather than nine-coordinate, since two of the halides are further away from M than the other seven. We have chosen to locate $PbCl_2$, therefore, between the seven-coordinate SrI_2 structure and the eight-coordinate CaF_2 systems (Figure 8).

The molecules that are linear in the gas phase form solids with CN = 4 or 6 (see Table 5), and with X−M−X angles ranging from the tetrahedral angle in the Be structures to 90° at the octahedrally coordinated Mg and Ca metal centers (Figure 8). The molecules that are bent in the gas-phase condense to give higher coordination solids (Table 5), with smaller X−M−X angles (between 70° and 80°) (Figure 8). The smallest angle X−M−X angles in the solids (~70.5°) is found in the fluorite structures (Figure 8). This structure type is the one adopted by systems such as SrF_2, BaF_2, and $BaCl_2$ for which the corresponding MX_2 gas-phase monomers (Table 1) and M_2X_4 dimers (Table 3) exhibit significant bending as well (see blue section in Table 6).

The relationship between the structural variation in the monomer and the solid crystal structures has been examined in further detail by reference to the linearized bending force constant k_{lin} of the metal dihalide monomers.

Since k_{lin} (see definition above) is sensitive to both the shape and flexibility of the molecule, it is an ideal index to employ in comparing the geometric trends. The bending force constants have a key advantage over the bond angle data in this regard. The bond angle provides no direct information about the degree of flexibility of the molecule, i.e., whether the potential minimum is shallow or deep. For molecules with similar bond angles, the bending force constants may vary over a large range (see Table 1 and Table S.2).

Shown in Figure 9 is a distribution of the MX_2 structure types and coordination numbers of the alkaline-earth dihalide solids at ambient conditions. The coordination numbers for all the structures are indicated in five columns, with one column for all the halides of each metal atom (Be−Ba). In each column, the four structures are spaced along the *y*-direction by the linearized bending force constant (Table 1) of the associated monomer.

In examining the splitting pattern in k_{lin} and the variation in the MX_2 crystal structure types (Figure 9), we were surprised by the apparent link between the two sets of data. As indicated in Table 6, as well, the linear gas-phase molecules condense to form either four- or six-coordinate solids. The higher coordination solids are preferred as the monomers become more flexible (as $k_{lin} = 0$ is approached), with the unique seven-coordinate SrI_2 and the $SrBr_2$ structures appearing in this region. Curiously, these two most nontypical MX_2 structure types are derived from two of the most flexible molecules among the group 2 dihalides.

All the CaF_2 (CN = 8) or the $PbCl_2$ (CN = 7 + 2) structure types fall in the region where k_{lin} is negative; i.e., only the bent alkaline earth metal halides condense to form the high coordination CaF_2 and genuine $PbCl_2$ structure types (blue section in Table 6). Hence, a partitioning of the crystal structures on the basis of coordination numbers and/or structure type separates solids for which the associated monomers are linear from those for which the associated monomers are bent.

A Traceable Connection?

In extended solids, a number of additional interactions that are irrelevant to gas-phase structures become important, such as the van der Waals interactions between layers in the $CdCl_2$ and CdI_2 structure types (Figure 7). Other interactions are diminished in influences; cation core-polarization effects disappear or become negligible at metal sites with high local

(59) Bracket, E. B.; Bracket, T. E.; Sass, R. L. *J. Phys. Chem.* **1963**, *67*, 2132.

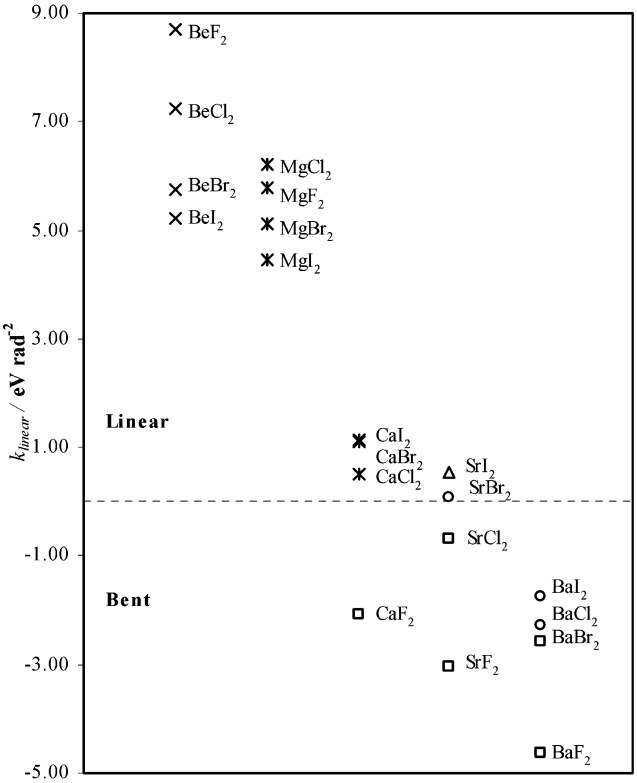

Type	Crystal
SiO_2	BeF_2
SiS_2	$BeCl_2$, $BeBr_2$, BeI_2
TiO_2	MgF_2
$CdCl_2$	$MgCl_2$
CdI_2	$MgBr_2$, MgI_2, CaI_2
$CaCl_2$	$CaCl_2$, $CaBr_2$
SrI_2	SrI_2
$PbCl_2$	$SrBr_2$, $BaBr_2$, BaI_2
CaF_2	CaF_2, SrF_2, $SrCl_2$, BaF_2, $BaCl_2$

Figure 9. Relationship between structure types (and cation coordination number) in MX_2 crystals and the geometry of MX_2 monomer in the gas phase; CN = 4 (×); CN = 6 (∗); CN = 7 (△);CN = 7+2 (○); CN = 8 (□). The bending force constants used are those listed in Table 1.

symmetry, as in the case of the eight-coordinate metal site in the fluorite structure (Figure 7). One might suppose, therefore, that the influences that are decisive in the monomers and dimers become less significant in higher order oligomers and the solids. Nonetheless, we have found that the linear and the bent monomers condense to form significantly different structure types. Further, the systems that exhibit exceptional behavior in the monomer or dimer forms, such as the very floppy $SrBr_2$, show exceptional behavior (a distorted $PbCl_2$ structure) in the solid phase as well.

We have shown above that although there is an important correlation, the structural variations in the dimers are not directly controlled by the linear/bent structural preferences in the monomer. The dimerization process is highly exothermic, and the dimerization energies are quite large compared to the computed monomer linearization energies (see Tables 1 and 4). Similarly, crystal packing forces in the solids are certainly likely to overcome the relatively weak deformation or preparation energies in the monomers. So, the geometry of the group 2 dihalide monomers, per se, is quite unimportant in determining the structure types of the corresponding solids. But what then is the common thread linking the structural preferences in the monomers, their dimers, and the solids?

As pointed out above, the feasibility of sd^x hybridization in Ca, Sr, and Ba is believed to be decisive for the geometric patterns in both the monomers and the dimers. The preference for higher coordination in the solids as M gets larger may be explained, as well, by the availability of lower lying *d*-orbitals for bonding. The availability of the $(n-1)d$ orbitals is important for explaining the high coordination and small angles in the fluorite and $PbCl_2$ structures, for example. The unavailability of the *d* orbitals in Be and Mg helps to explain the lower four- and six-coordination in the Be and Mg systems. The increase in CN from BeX_2 to BaX_2 across each row of Table 6 can be rationalized, therefore, in a straightforward manner.

How, though, are the variations down the columns in Table 6 to be explained? The decreased bending of the dihalide molecules as X gets larger has been accounted for partly by the dependence of the sd^x-hybridization at M on the electronegativity of X. Based on the work of Cruickshank et al.,[60] Coulson pointed out that separation between the *s* and $(n-1)d$ orbitals in M is expected to decrease as the ionic character of the M−X bond increases.[8] So, participation of the *d* orbital in bonding is expected to be greatest for X = F and least for X = I. Since the $s \rightarrow d$ excitation energy decreases anyway in going from Ca to Ba, the influence of the halides on the sd^x-hybridization should be more important for Ca compared to Sr and Ba. The electronegativity of X will be more decisive for the involvement of *d* orbitals in CaX_2 (monomer, dimer or solid) systems than it will be for the SrX_2 and BaX_2 systems. So, for instance, while only CaF_2 is bent in the CaF_2 to CaI_2 series, both SrF_2 and $SrCl_2$ and all the Ba dihalides are bent.

It is interesting that as we go down the Ca, Sr, and Ba columns in Table 6 the coordination numbers (and structure types) of the solids follow an analogous pattern: only CaF_2 in the Ca series has CN > 7, while SrF_2, $SrCl_2$, $SrBr_2$, and all the Ba dihalides have CN > 7. Might the decreased separation of the *s* and *d* orbitals as X gets more electronegative also play a role in rationalizing that behavior?

(60) Cruickshank, D. W. J.; Webster, B. C.; Mayers, D. F. *J. Chem. Phys.* **1964**, *40*, 3733; **1964**, *41*, 325 (erratum).

Classically, the decreased coordination number in the Ca structures as X gets larger has been explained in terms of hard sphere repulsion (steric effects) limiting the number of halides that can congregate around a metal center. Pauling's first rule, stipulating a connection between the cation/anion radius ratio and cation coordination number (ref 24a, p 44), is in line with that analysis. The role of sd^x-hybridization has not been cited before to explain details of the structure type preferences in these or any other system.

Summary and Outlook

Links between the structural variations of some group 2 dihalide molecules and their dimers have been noted previously. Our desire to probe these connections and to inquire whether the extended solids of the group 2 dihalides (BeX_2 to BaX_2) "remember" the gas-phase structures has motivated a comprehensive examination of structural preferences in the monomers, dimers, and solids.

We find some remarkable correlations between the linear-(bent) geometry in the MX_2 monomers, the $D_{2h}(C_{3v})$ M_2X_4 structural preferences in the dimer, and the structure type preferences in the MX_2 extended solids.

The rigid linear monomers show a strong preference for forming the D_{2h} doubly bridged structure and condense to form at ambient conditions extended solids with low coordination numbers CN = 4, 6. The monomers that are bent strongly prefer the C_{3v} triply bridged dimer geometry and condense to form extended solids (in the $PbCl_2$ and fluorite structure types) that have high coordination numbers (CN = 7 + 2, 8). The quasilinear or floppy monomers form either the D_{2h} or the C_{3v} dimer, with a relatively low barrier separating the two isomers. Two of the very floppy molecules, $SrBr_2$ and SrI_2, form unique extended solids at ambient conditions.

The structural preferences in the dimers have been rationalized partly by an MX_2 frontier orbital MO analysis based on sp^x hybridization. The strong preference for the D_{2h} structure in the Be and Mg dihalide dimers is explained by the large cost in energy required to deform the linear MX_2 fragments for optimal bonding in the C_{3v} geometry. The C_{3v} dimer structure is favored only when the cation is very large, especially when the minimum energy structure of the MX_2 monomer is bent.

The bending in the MX_2 monomer has been explained previously by core-polarization interactions between M and X sites and the availability of *d*-orbitals on M for hybridization with the valence *s* orbitals. We believe the significant stabilization of the C_{3v} geometry for the CaX_2, SrX_2, and BaX_2 dimers may be rationalized, as well, both by core-polarization effects, as the metal gets softer going from Be to Ba, and by the availability of *d*-orbitals in Ca, Sr, and Ba.

Polarization effects play a smaller role in the MX_2 extended solids. In addition to the usual rules explaining structure type preferences in ionic solids, we consider that the observed high coordination in CaF_2 and the strontium and barium dihalide solids (Tables 5 and 6) is consistent with the accessibility of the *d*-orbitals at the metal sites and a reduction in the $ns-(n-1)d$ energy separation as X gets more electronegative.

While we are happy with the degree of understanding we have reached, a number of new questions have arisen in this study that deserve further analysis. Given the size and diversity of the structures in the group 2 dihalides, we have been obliged to focus in this work on the set of monomers, dimers, and infinite extended solids. In the future, we would like to consider, as well, the structural preferences (in the gas and solid phases) of transition metal dihalides. In particular, we are interested in examining the bonding patterns in the group 12 dihalides. Much work remains to be done.

Acknowledgment. We are grateful to Cornell University for its support of this research, and to Magdolna Hargittai for some important comments and references. Computational resources were kindly provided by the Cornell NanoScale Facility, a member of the National Nanotechnology Infrastructure Network, which is supported by the National Science Foundation (Grant ECS 03-35765).

Supporting Information Available: Experimental and computed (B3LYP, MP2 and QCISD) minimum energy geometries of the group 2 dihalides; Optimized bond distances for the group 2 dihalides in the linear conformation, linearization energies for the bent dihalides, and the computed bending force constants for the linear molecules; Relative energies obtained at the B3LYP level for all the dimer isomers studied (Figure 2) and the number of imaginary frequencies for each isomer; MP2 geometries of the D_{2h} and C_{3v} dimers; B3LYP vibrational frequencies obtained for the D_{2h} and C_{3v} dimer structures; Computed deformation (preparation) and dimerization energies (E_{def} and E_{dim}) for the MX_2 fragments of the D_{2h} and C_{3v} group 2 dihalide dimers; Complete bibliographic citation of ref 32 in the text. This material is available free of charge via the Internet at http://pubs.acs.org.

JA062817J